AIAA 92-0020

Computational Investigation Of Slot Blowing For Fuselage Forebody Flow Control

Scott M. Murman
MCAT Institute, NASA Ames Research Center

Yehia M. Rizk
NASA Ames Research Center

Russell M. Cummings
California Polytechnic State University, San Luis Obispo

Lewis B. Schiff
NASA Ames Research Center

30th Aerospace Sciences Meeting & Exhibit
January 6-9, 1992 / Reno, NV

Computational Investigation of Slot Blowing for Fuselage Forebody Flow Control

Scott M. Murman *
MCAT Institute, Moffett Field, CA 94035

Yehia M. Rizk †
NASA Ames Research Center, Moffett Field, CA 94035

Russell M. Cummings ‡
California Polytechnic State University, San Luis Obispo, CA 93407

Lewis B. Schiff +
NASA Ames Research Center, Moffett Field, CA 94035

ABSTRACT

This paper presents a computational investigation of a tangential slot blowing concept for generating lateral control forces on an aircraft fuselage forebody. The effects of varying both the jet width and jet exit velocity for a fixed location slot are analyzed. This work is aimed at aiding researchers in designing future experimental and computational models of tangential slot blowing. The primary influence on the resulting side force of the forebody is seen to be the jet mass flow rate. This influence is insensitive to different combinations of slot widths and jet velocities over the range of variables considered. Both an actuator plane and an overset grid technique are used to model the tangential slot. The overset method successfully resolves the details of the actual slot geometry, extending the generality of the numerical method. The actuator plane concept predicts side forces similar to those produced by resolving the actual slot geometry.

NOMENCLATURE

b = *width of tangential slot*
$\bar{c}$ = mean aerodynamic chord of F-18 wing = 11.25 ft.
h = time step = Δt
i_b = iblank array = 0 at hole points, 1 at interior points
$\dot{m}$ = mass flow rate, lbm/sec
n = normal distance from the wall
p = static pressure
q = freestream dynamic pressure = $\frac{1}{2}\rho V^2$
x, y, z = cartesian body coordinates
y^+ = turbulent shear stress length
z = longitudinal distance from slot exit plane
z^* = longitudinal distance from slot exit plane to position of $C_{p=\frac{1}{2}(C_{p_{max}} - C_{p_{min}})}$
$\hat{A}, \hat{B}, \hat{C}$ = linearized inviscid flux vectors
C_l, C_m, C_n = rolling- pitching- and yawing-moment coefficients = $\frac{\text{moment}}{q_\infty S_{ref} \bar{c}}$
C_p = static pressure coefficient
C_X, C_Y, C_Z = axial- side- and normal-force coefficients = $\frac{\text{force}}{q_\infty S_{ref}}$
C_μ = jet momentum coefficient = $\frac{\dot{m}_j V_j}{q_\infty S_{ref}}$
D_e, D_i = explicit, implicit numerical dissipation
$\hat{E}, \hat{F}, \hat{G}$ = inviscid flux vectors
I = identity matrix
L = slot length
M = Mach number
$\hat{M}$ = linearized surface-normal viscous flux vector
$\hat{Q}$ = vector of conserved variables
Re = Reynolds number = $\frac{VL}{\nu}$
Re_j = Reynolds number = $\frac{V_j b}{\nu_j}$
S_{ref} = F-18 wing reference area = 400 sq. ft.
T = temperature
$\hat{T}$ = surface-normal viscous flux vector
V = velocity
α = angle of attack
δ = finite-difference operator
ρ = density
θ = boundary layer momentum thickness
ξ, η, ζ = computational body-fitted coordinates

Subscripts

j = jet conditions
∞ = freestream conditions

I. INTRODUCTION

The typical flowfield around modern fighter aircraft at moderate-to-high angles of attack is dominated by highly energetic vortices. The F-18 utilizes wing leading edge extensions (LEX) to generate vortices which enhance the wing lift, and the twin vertical tails are canted to intercept the strong vortex field and increase maneuverability. As the angle of attack of the aircraft increases, the yaw power required for maneuvering also increases. At large incidence the LEX vortices burst upstream of the vertical

---

* Research Scientist, formerly Graduate Research Assistant, Aeronautical Engineering Department, California Polytechnic State University, San Luis Obispo, CA.

† Research Scientist, Applied Computational Fluids Branch. Associate Fellow, AIAA.

‡ Professor, Aeronautical Engineering Department. Associate Fellow, AIAA.

+ Special Assistant for High Alpha Technology, Fluid Dynamics Division. Associate Fellow, AIAA.

tails, resulting in a loss of yaw control power. The main emphasis of vortical flow control is to provide additional yaw control power at high angles of attack to augment that generated by the existing empennage.

Within NASA, the High Alpha Technology Program is currently studying several methods of providing additional yaw power at high angles of attack. These include the use of thrust vectoring,[1] and forebody flow control concepts including actuated forebody strakes[2] and pneumatic forebody flow control.[3] The forebody control concept examined in this study consists of a pneumatic control system where air is ejected tangentially to the body surface from a thin slot located on the radome of the F–18. Tangential slot blowing creates a wall jet which effectively moves the primary forebody crossflow separation line (Fig. 1). This alteration of the forebody flowfield interacts with previously existing flow structures to create forces and moments to control the aircraft. The present study considers only the isolated F–18 forebody, from the nose to the leading edge of the wing.

The current work utilizes Reynolds-averaged Navier-Stokes flow computations to investigate the effects of variable slot widths and jet exit velocities on a fixed location tangential slot. The study is aimed at providing data which cannot be extrapolated from current experimental results, thus aiding experimental researchers in designing future test models. Further, computational considerations specific to slot blowing are addressed. The use of a Chimera zonal approach[4] to model the tangential slot is investigated and compared to an actuator plane slot simulation.[5] The Chimera method provides a modular computational tool suitable for inclusion in general full-aircraft computations or turbulence modeling studies. The actuator plane concept can simplify the grid generation procedure while giving accurate engineering results.

The governing equations and numerical method are described in Section II of this paper, while the results are presented in Section III. Section IV briefly summarizes the results and presents recommendations for future work.

II. NUMERICAL METHOD

Part of this study contrasts two methods of simulating slot blowing computationally: using an actuator plane concept, and resolving the actual slot geometry using an overset grid technique. Both methods utilize the same basic numerical algorithm with some minor differences in application. These differences will be noted where applicable, and a full description of the two methods is given in the Slot Definition section.

Governing Equations And Numerical Algorithm

For high-Reynolds-number flows, the use of a body-fitted coordinate system allows the full Reynolds-averaged Navier-Stokes equations to be simplified by using the thin-layer approximation.[6] Maintaining the viscous terms in only the surface-normal direction, the governing equations take the following conservative form

$$\partial_\tau \widehat{Q} + \partial_\xi \widehat{F} + \partial_\eta \widehat{G} + \partial_\zeta \widehat{H} = Re^{-1}\partial_\zeta \widehat{T} \qquad (1)$$

where $\widehat{Q}$ represents the dependent variable vector, $\widehat{F}$, $\widehat{G}$, and $\widehat{H}$ are the inviscid flux vectors, and $\widehat{T}$ contains the remaining viscous terms.

The above equations are numerically integrated using the F3D code, an implicit two-factor scheme that uses central differencing in the η and ζ directions and upwind differencing in the ξ direction. The discretized form of Eq. 1 is

$$\begin{aligned}\mathcal{L}_f\mathcal{L}_b\Delta\widehat{Q}^{n+1} = \\ -i_b\Delta t\Big\{\delta_\xi^b(\widehat{F}^+)^n + \delta_\xi^f(\widehat{F}^-)^n + \delta_\eta\widehat{G}^n + \delta_\zeta\widehat{H}^n \\ - Re^{-1}\bar{\delta}_\zeta\widehat{T}^n - (D_e|_\eta + D_e|_\zeta)\widehat{Q}^n\Big\}\end{aligned} \qquad (2)$$

where the forward and backward operators, $\mathcal{L}_f$, $\mathcal{L}_b$ are given by

$$\mathcal{L}_f = I + i_b\Big\{h\delta_\xi^b(\widehat{A}^+)^n + h\delta_\zeta\widehat{C}^n - hRe^{-1}\bar{\delta}_\zeta J^{-1}\widehat{M}^n J - D_i|_\zeta\Big\}$$

and

$$\mathcal{L}_b = I + i_b\Big\{h\delta_\xi^f(\widehat{A}^-)^n + h\delta_\eta\widehat{B}^n - D_i|_\eta\Big\}$$

In the current work, solutions are obtained in a steady-state mode where local time stepping is used to speed up convergence. In Eq. 2, $h = \Delta t$, where Δt is the time step which is allowed to vary from point to point according to a function of the Jacobian of the coordinate transformation. Also, δ is a three-point second-order-accurate central-difference operator, while $\bar{\delta}$ is a midpoint operator used with the viscous terms. The flux $\widehat{F}$ associated with the ξ direction has been eigensplit allowing the use of backward- and forward-difference operators δ_ξ^b and δ_ξ^f. The matrices $\widehat{A}$, $\widehat{B}$, $\widehat{C}$, $\widehat{M}$, and $\widehat{N}$ result from local linearization of the fluxes about the previous time level. Further details on the development of the algorithm can be found in Refs. 7 and 8.

The only difference between Eq. 2 and the algorithm as applied to the actuator plane cases is the introduction of the integer array i_b. This array allows the use of overset grids and takes the value of one at regular field points, and zero at boundary or hole points. When $i_b = 1$, Eq. 2 reduces to the original algorithm, while when $i_b = 0$ the right hand side is zero and the scheme reduces to $\widehat{Q}^{n+1} = \widehat{Q}^n$. In the actuator plane implementation $i_b = 1$ everywhere and the zonal communication is specified explicitly.

Explicit and implicit numerical dissipation terms (D_e and D_i in Eq. 2) are introduced in the η and ζ directions to suppress the high frequencies associated with central differencing. The implicit smoothing consists of only second-order terms, while the explicit smoothing uses a blend of second- and fourth-order terms. The introduction of i_b in the explicit smoothing causes the overset scheme to switch from fourth-order to second-order adjacent to blanked-out regions (Ref. 9).

Slot Definition

Both the actuator plane and actual geometry approaches utilize the same base F–18 forebody grid. The original grid is a two-zone C-O type grid consisting of one zone for the forebody and another for the LEX region. This

grid configuration contains approximately 500,000 points, with the first grid line above the body surface located at $y^+ \approx 5$. The forebody extends from the nose to the wing leading edge of the aircraft, a distance of 29.15 ft. These dimensions correspond to the full-scale dimensions of the aircraft. The grid extends approximately one body length from the surface in all directions except downstream of the body. This grid definition was previously used for isolated forebody calculations without blowing,[10] and was shown to give an accurate resolution of the main flow features.

Actuator Plane

The actuator plane concept is a straightforward approach to slot blowing designed to simplify the grid generation and solution procedure. If one assumes that the momentum and energy of the jet are much greater than those of the incoming boundary layer at the slot lip, then it can be argued that the location of the wall jet separation will be determined primarily by the jet parameters[5]. The actuator plane concept is illustrated schematically in Fig. 2. Rather than resolve the details of the geometry and jet/boundary layer interaction, the incoming boundary layer is simply overwritten with the mass, momentum, and energy of the jet. In order to apply the actuator plane, existing grid lines must be chosen to define the slot length and width. The plane which contains these lines is chosen to divide the original grid into two sub-zones, and the jet parameters are specified as explicit boundary conditions. Details on the actuator plane method as utilized in the current work can be found in Refs. 5 and 11.

Actual Geometry

The resolution of the actual slot geometry is accomplished using the Chimera grid-embedding technique. The method simplifies the construction of computational grids about complex geometries by dividing the physical domain into regions which can accommodate easily-generated grids. This results in an overset grid method which requires only that neighboring grids overlap each other. In order to extend the capabilities of the overset method to include regions which overlap only slightly, the current implementation can also function in a blended overset and patched mode (Ref. 12). The Pegasus code[4] is used to establish communications between the interconnecting grids and to remove any unwanted regions ("hole points"). All boundary values are updated explicitly at each iteration by trilinear interpolation. Like other general zonal methods, the overset/patched method provides the capability of using different grid densities, flow solvers, or turbulence models in different regions of the flow depending upon physical considerations.

In the current study, a tangential slot beginning 0.4 ft. behind the nose and extending downstream for 3.6 ft. is used. The slot is located circumferentially approximately 90° from the windward symmetry plane. This configuration is similar to an experimental configuration recently tested in the NASA Ames 80 x 120 ft. wind tunnel. The grid line that defines the slot length and circumferential location is common to both the actuator plane and the actual geometry implementations. The streamwise cross-sections for the actual geometry resolution cases are modeled after the NASA wind tunnel configuration. The blending is done from the end of a vertical slot wall to a specified point on the forebody using a constant radius arc that passes between the two points (Fig. 3). The height of the vertical slot wall is dependent upon the local radius of curvature of the forebody, and is chosen to provide the smoothest surface.

Because a large portion of the slot grid actually lies interior to the forebody, care must be taken to ensure that numerical errors do not occur in the overset zonal communication. Anticipating this, the slot patch is kept small to facilitate the testing of many grids without having to rely on numerical grid generation procedures. The slot grid is clustered normal to the solid wall to resolve the viscous layers, and also at the junction of the forebody and the jet to resolve the slot lip. Figure 4 shows a typical grid cross section within the slot/forebody overlap region. Here every other radial grid line is shown for clarity. Due to computer memory limitations, and to accommodate the slot definition, the forebody grid is divided into a ten-zone configuration. A half-body view of this configuration is shown in Fig. 5.

Boundary Conditions

The outer boundaries of the computational domain are maintained at the undisturbed freestream conditions, and a zero-axial-gradient extrapolation is used at the downstream edge. The solid wall conditions are specified as no-slip, adiabatic wall, and $\left(\frac{\partial p}{\partial n}\right)_w = 0$.

In order to compare directly with previous computations, the jet-exit boundary conditions are implemented in both slot simulation methods in a manner similar to previous actuator plane studies. In this method the density and pressure at the jet exit plane are approximated as the freestream conditions, and the tangential velocity of the jet is then specified to obtain the vector of conserved quantities $\widehat{Q}$. For subsonic flow, this method overspecifies the boundary conditions, and a small discontinuity normally exists at the jet exit plane.

Turbulence Modeling

In the current work, computations are carried out at high Reynolds number flight conditions. This produces turbulent flow over the majority of the forebody, with the exception of a small laminar and transitional region near the nose. This region is neglected and the computations are performed assuming the flow to be fully turbulent. The algebraic turbulence model of Baldwin and Lomax[13] , with modifications for crossflow separation due to Degani and Schiff[14] , is used throughout the flowfield. This combination provides a computationally efficient model that has been used extensively in three-dimensional high-incidence problems with good success.

The physics of the turbulent jet flows considered in this work is extremely complex. Jets of variable strength and thickness, flowing over curved surfaces of varying cross-sections, and in the presence of both favorable and adverse pressure gradients, exist. Unfortunately, a turbulence model to handle this type of flow has not been validated. Without detailed experimental data to use as a guide, extrapolating a simplified jet turbulence model to such a complicated flow may lead to significant errors and is beyond the scope of this work. The Baldwin-Lomax turbulence model was maintained in the jet region because of its simplicity.

III. RESULTS AND DISCUSSION

Navier-Stokes simulations of tangential slot blowing were obtained for the isolated F–18 forebody. The flow conditions in all cases are $M_\infty = 0.2$, $\alpha = 30.0°$, and $Re_{\bar{c}} = 11.52 \times 10^6$, where $\bar{c}$ is the mean aerodynamic chord of the wing. These conditions represent typical high-angle-of-attack flight-test conditions, and have been used in previous F–18 computational studies (cf. Refs. 5, 12, and 15). The discussion begins with two no-blowing cases which are used to illustrate the main features of the forebody flowfield and provide the baselines for comparison with the blowing cases. Further sections discuss different computational and physical considerations pertinent to tangential slot blowing.

Geometry Resolution vs. Actuator Plane Concept

No-Blowing Computations

The no-blowing flowfield about the F–18 fuselage forebody considered in this work has been previously analyzed. Numerical simulations have been performed,[10,16] and flight-test data was obtained using the High Alpha Research Vehicle (HARV). The two no-blowing solutions reported here, one including the slot geometry and one with a "smooth" forebody, are computed starting from the solution of Ref. 10 using the overset numerical method. The computed solution without the slot geometry included is essentially identical to that reported in Ref. 10. Including the slot geometry results in an 8 % increase in the computed normal force, and negligible changes in the axial and side forces on the forebody, compared to the smooth forebody geometry.

Including the slot geometry changes the surface flow pattern in the region of the slot (Fig. 6). In both the actual geometry and actuator plane cases, a primary crossflow separation line forms upstream of the LEX, with a corresponding secondary forebody separation forming close to the leeward symmetry plane. When the slot geometry is included, differences in the surface topology can be seen upstream of the LEX (Fig. 6b). In the slot region, the flow separates at the slot lip and reattaches leeward, causing the primary forebody crossflow separation line to move slightly leeward. The flow over the forward wall of the slot also separates, causing the primary and secondary separation lines to reform downstream. Aft of the slot, the forebody separation regions are located further leeward when the slot geometry is included. In this computation, the slot face (the region where blowing would normally be implemented) is considered closed, and solid wall boundary conditions are imposed. Except at the ends of the slot, the flow is nearly identical to the flow over a backward facing step. In Fig. 7, the wall static pressures at three axial locations within the slot region are compared with experimental data for a two-dimensional, turbulent flow over a backward-facing step on a flat plate (Ref. 17). This correlation suggests that even in this three-dimensional flow, the interactions near the slot lip of this configuration may be amenable to a two-dimensional analysis. Specifically, the use of a two-dimensional turbulence model for the jet/boundary layer interactions may be applicable.

Blowing Computations

Table 1 summarizes the blowing cases computed, together with the labels which are used for reference. The computed force and moment coefficients are also given in Table 1. In all force calculations only the contribution of pressure is considered, and the moments are taken about a center located at the downstream end of the computational domain, as was done in Refs. 11 and 15. The mass flow rates and blowing coefficients for the similar actuator plane and geometry cases differ. This is mainly due to the differences in the jet velocity profile caused by resolving the slot lip (cf. Figs. 2 and 3), and the solid walls located at the upstream and downstream edge of the slot when the geometry is resolved. In all cases the blowing is initiated from the pilots' right side only. In the actual geometry cases the pilots' left side slot is also resolved, however it is considered closed and solid wall boundary conditions are imposed.

For reasons to be discussed in the next section, comparison of the actuator plane concept and overset slot grid resolution methods will concentrate on the two cases with the closest mass flow rates, cases G4 and A1. In all cases computed, the momentum and energy of the jet are much greater than those of the incoming boundary layer. This is the fundamental assumption used to justify employing an actuator plane to simulate tangential blowing. The results indicate that this is applicable for the jet conditions computed. The actuator plane case A1 has a slightly higher jet mass flow rate, and the resulting side force coefficient is approximately 2 % greater than that obtained in the actual geometry case G4. However, the yawing moment coefficient is slightly smaller in the actuator plane case. This is explained by examining the side-force distributions along the forebody for the two cases (Fig. 8). The distribution is similar for the two methods except in the slot region (the region denoted by circumferential lines on the forebody). The jet flow in the actuator plane case develops less side force than the actual geometry case. Because the majority of the force production is seen to come from the LEX region, the net side forces show consistent differences. However, the long moment arm from the moment center to the slot magnifies the differences in force production in the slot region when yawing moment is considered. For this reason, the following discussions will concentrate on the side force production.

The surface flow patterns for these two cases (Fig. 9), show that the topologies contain small differences near the slot region, consistent with the comparison of the no-blowing flowfields and the distributions of side force. Blowing on the right-hand side causes the wall jet to attach to the body, and the jet separation line moves across the leeward symmetry plane. In the actuator plane method the separation line moves farther than with the overset method. This behavior is representative of each actuator plane case computed, and affects the production of side force within the slot region. On the left-hand side, opposite the blowing slot, the separation-reattachment region windward of the jet separation forms in nearly the same azimuthal location in both cases. The modeling of the backward facing step on the left side causes this separation to form closer to the nose in the overset cases, again creating differences in force production within the slot region between the two methods. In the LEX region, the sharp leading edge fixes the separation line location, and consequently the flowfield above the LEX is essentially the same in both cases.

Figure 10 shows the corresponding helicity density contours[18] and local streamlines for cases G4 and A1. In this figure, light shades of gray represent clockwise vor-

tex rotation when viewed from the nose, and dark shades denote counter-clockwise rotation. The vortex that forms when the wall jet separates from the forebody lifts high off of the body and remains on the left-hand side in both cases. Consistent with the surface flow patterns, the main features of the flowfield in both cases are identical. The jet vortex is displaced slightly further outboard in case A1. This is again representative of each actuator plane case computed in this study.

One minor difference between the results obtained from the overset and the actuator plane methods is observed on the body surface at the jet exit. A crossflow separation line forms midway down the length of the slot when the geometry is resolved (Fig. 11a). The same topology also occurs in the actuator plane cases, however it occurs above the body, at the top edge of the slot, and consequently it is not observed in the surface flow pattern of Fig. 11b. This separation is believed to be a non-physical result caused by the jet-exit-plane boundary conditions. The pressure in the boundary layer approaching the slot is less than the freestream pressure, whereas the jet is fixed at the freestream pressure. For a sufficiently blunt body, this imposed adverse circumferential pressure gradient becomes significant and leads to the observed separation.

While the use of an actuator plane to simulate the slot simplifies the solution process, the technique does have limitations. The actuator plane must lie along lines of the existing forebody grid, and the number of possible configurations is restricted. Further, a grid clustering specific to attached boundary layer flows, rather than one optimized for the jet flow, is used. On the other hand, with the use of the Chimera overset technique arbitrary grids can be placed anywhere on the forebody. This flexibility is useful in grid resolution or grid adaptation studies. The two methods require approximately the same amount of computational time. The creation of sub-zones to apply the actuator plane concept reduces the efficiency of the implicit numerical algorithm, however the additional grid points required to model the slot using the Chimera technique also increases the required computational time. In general, it is felt that the resolution of the slot geometry using an overset technique adds significant flexibility to the numerical procedure, while the actuator plane method can give accurate engineering predictions without employing relatively complex grid embedding techniques.

Configuration Optimization

Computational investigations of slot blowing for pneumatic forebody flow control[5,11,15] have concentrated on the effectiveness of slots with different lengths and locations, having a fixed slot width and fixed jet exit velocity. However, experimental investigations of trailing-edge slot blowing as a means of increasing the lift of an airfoil suggest that decreasing the width of the slot can provide comparable efficiencies (Ref. 19). This study investigates the effects of variations in slot width and jet velocity on a fixed length and fixed location slot for tangential blowing.

Figure 12 shows the computed net side-force coefficient as a function of C_μ, the jet momentum coefficient, for all cases computed. Previous experimental and computational studies have tended to use C_μ as the relevant similarity parameter. In the current computations where varying slot widths were investigated, C_μ did not prove to be the governing parameter. It is seen from Fig. 12 that the same value of jet momentum coefficient can give different values of side force, depending upon the width of the slot. However, upon replotting these same cases with jet mass flow rate $\dot{m}_j$ as the independent parameter, a linear correlation is observed within the range of mass flow rates investigated (Fig. 13). From Table 1, it can be seen that the net forces are nearly identical between cases G2 and G3, two cases having identical mass flow rates and different values of C_μ.

It is apparent from Fig. 13 that $\dot{m}_j$ is the driving parameter, independent of the combination of slot thicknesses and jet velocities, over the range of variables considered. However, the current computations were performed at only one freestream condition, and the behavior for other flow conditions should be investigated. The jet mass flow rate is a dimensional quantity and would not be useful for correlating other freestream conditions. To nondimensionalize $\dot{m}_j$, note that the jet mass flow rate is proportional to a jet Reynolds number, i.e. $\dot{m}_j = L\mu_j Re_j$, where $Re_j = \frac{U_j b}{\nu_j}$. Use of Re_j/Re_θ, the ratio of jet Reynolds number to the Reynolds number of the incoming boundary layer, may provide a more consistent measure of blowing effectiveness than C_μ. For most applications this quantity should be $\mathcal{O}(1)$, and the introduction of the oncoming boundary layer profile could allow different flow conditions to be directly compared.

The effect of increasing the mass flow rate is most easily seen in the distribution of side force along the forebody. Figure 14 compares the integrated surface pressures at each axial location for cases G1, G4, A1, and A3. The difference in slot simulation again can be seen within the slot region, where the actuator plane case consistently provides less side force because of the delayed separation. Downstream of this region, the incremental changes with mass flow rate produce consistent incremental changes in side force along the length of the forebody. In the slot region this behavior is seen within each method of simulating the slot. In all cases the majority of the net side force is developed in the LEX region. Even though large asymmetries are not visible in the LEX vortex flowfield (Fig. 9), the interactions of the imposed asymmetric jet vortex structure with the strong LEX vortices cause significant force production. The wall jet vortex with a greater amount of mass appears to interact to a greater extent, and the pressure on the body surface is influenced accordingly.

IV. CONCLUSIONS

Navier-Stokes simulations for the isolated F-18 forebody were obtained to assess the accuracy of an actuator plane concept for simulating slot blowing, in comparison to an overset grid method which resolved the actual slot geometry. In addition, the effects of variations in slot width and jet velocity were investigated. The main conclusions can be summarized as follows:

1) The use of an actuator plane concept produced side force predictions similar to those produced by modeling the actual slot geometry for the jet flows considered.

2) The jet mass flow rate was the governing parameter for the side force production, independent of the combinations of slot widths and jet exit velocities, over the range of conditions investigated.

3) The jet momentum coefficient did not provide a consistent measure of the side force production when the slot width was varied.

4) An overset grid technique was successfully used to resolve the details of the actual slot geometry, extending the flexibility of the numerical method.

The effects of the altered vortex structure due to blowing on a complete aircraft, e. g. the effects of blowing on the LEX vortex breakdown, are not considered in the current work. The overset grid method can easily accommodate a slot definition into a full aircraft configuration, but more research into the jet simulation is necessary. The jet-exit-plane boundary conditions need to be refined to accurately model the physics involved. As experimental data becomes available, a suitable turbulence model can also be developed. Further, computational grid resolution studies on the wall jet and its separation need to be performed. The influence of the jet mass flow rate on the side force at different freestream conditions also warrants further investigation.

ACKNOWLEDGEMENTS

This work was partially funded by NASA Grant NCC2-564.

REFERENCES

[1] Bowers, A. H., Noffz, G. K., and Peron, L. R., "An Aerodynamic and Jet Deflection Model for Thrust Vectoring on the NASA F/A-18 High-Alpha Research Vehicle," NASA High-Angle-of-Attack Technology Conference, NASA Langley Research Center, October, 1990.

[2] Murri, D. G., Biedron, R. T., Erickson, G. E., Jordan, F. L., and Hoffler, K. D., "Development of Actuated Forebody Strake Controls for the F-18 High-Alpha Research Vehicle," NASA High-Angle-of-Attack Technology Conference, NASA Langley Research Center, October, 1990.

[3] Schreiner, J. A., Erickson, G. E., and Guyton, R., "Application of Tangential Sheet Blowing on the Forebody of an F-18-like Configuration for High-Angle-of-Attack Maneuverability," NASA High-Angle-of-Attack Technology Conference, NASA Langley Research Center, October, 1990.

[4] Benek, J. A., Steger, J. L., Dougherty, F. C., and Buning, P. G., "Chimera: A Grid Embedding Technique," AEDC-TR-85-64, Arnold Air Force Station, TN, 1986.

[5] Tavella, D. A., Schiff, L. B., and Cummings, R. M., "Pneumatic Vortical Flow Control at High Angles of Attack" AIAA Paper 90-0098, January, 1990.

[6] Steger, J. L., "Implicit Finite-Difference Simulation of Flow About Arbitrary Two-Dimensional Geometries," *AIAA Journal* **16** (1978), 679-686.

[7] Steger, J. L., Ying, S. X., and Schiff, L. B., "A Partially Flux-Split Algorithm for Numerical Simulation of Compressible Inviscid and Viscous Flow," Proceedings of a Workshop on Computational Fluid Dynamics, University of California, Davis, 1986.

[8] Ying, S. X., Steger, J. L., Schiff, L. B., and Baganoff, D., "Numerical Simulation of Unsteady, Viscous, High Angle of Attack Flows Using a Partially Flux-Split Algorithm," AIAA Paper 86-2179, 1986.

[9] Buning, P. G., Chiu, I. T., Obayashi, S., Rizk, Y. M., and Steger, J. L., "Numerical Simulation of the Integrated Space Shuttle Vehicle in Ascent," AIAA Paper 88-4359, August, 1988.

[10] Schiff, L. B., Cummings, R. M., Sorenson, R. L., and Rizk, Y. M., "Numerical Simulation of High-Incidence Flow over the F-18 Fuselage Forebody," AIAA Paper 89-0339, January, 1989.

[11] Tavella, D. A., Schiff, L. B., and Gee, K., "Fighter Yaw Control at High Incidence Through Fuselage Blowing," NASA High-Angle-of Attack Technology Conference, NASA Langley Research Center, October, 1990.

[12] Rizk, Y. M., and Gee, K., "Numerical Prediction of the Unsteady Flowfield Around the F-18 Aircraft at Large Incidence," AIAA Paper 91-0020, January, 1991.

[13] Baldwin, B. and Lomax, H., "Thin-Layer Approximation and Algebraic Model for Separated Turbulent Flows," AIAA Paper 78-0257, January, 1978.

[14] Degani, D. and Schiff, L. B., "Computation of Turbulent Supersonic Flows About Pointed Bodies Having Crossflow Separation," *J. Comp. Phys.* **66** (1986), 173-196.

[15] Gee, K., Tavella, D., and Schiff, L. B., "Computational Optimization of a Pneumatic Forebody Flow Control Concept," AIAA Paper, 91-3249, September, 1991.

[16] Ghaffari, F., Luckring, J., Thomas, J., and Bates, B., "Navier-Stokes Solution about the F/A-18 Forebody-LEX Configuration," AIAA Paper, 89-0338, January, 1989.

[17] Narayanan, M. A. B., Khadgi, Y. N., and Viswanath, P. R., "Similarities in Pressure Distribution in Separated Flow Behind Backward-Facing Steps," *Aero. Quarterly* **25** (1974), 305-312.

[18] Levy, Y., Degani, D., and Seginer, A., "Graphical Visualization of Vortical Flows by Means of Helicity," *AIAA Journal* **28** (1990), 1347-1352.

[19] Wood, N. and Nielson, J., "Circulation Control Airfoils Past, Present, and Future," AIAA Paper 78-0257, January, 1978.

SLOT DEFINITION	LABEL	b (in.)	M_j	$\dot{m}_j$ (lbm/s)	C_μ	C_X	C_Y	C_Z	C_l	C_m	C_n
GEOMETRY	G1	0.13	0.72	1.04	0.0021	-.018	.063	0.45	-.0009	0.35	.066
GEOMETRY	G2	0.17	0.63	1.19	0.0021	-.018	.065	0.45	-.0013	0.35	.068
GEOMETRY	G3	0.13	0.82	1.19	0.0027	-.018	.065	0.44	-.0022	0.35	.070
GEOMETRY	G4	0.17	0.72	1.35	0.0027	-.018	.069	0.45	-.0020	0.35	.073
ACTUATOR	A1	0.13	0.72	1.43	0.0028	-.019	.070	0.45	-.0014	0.36	.070
ACTUATOR	A2	0.17	0.63	1.60	0.0028	-.020	.073	0.45	-.0020	0.36	.074
ACTUATOR	A3	0.17	0.72	1.82	0.0036	-.021	.078	0.45	-.0019	0.36	.079

Table 1. Summary of blowing computations

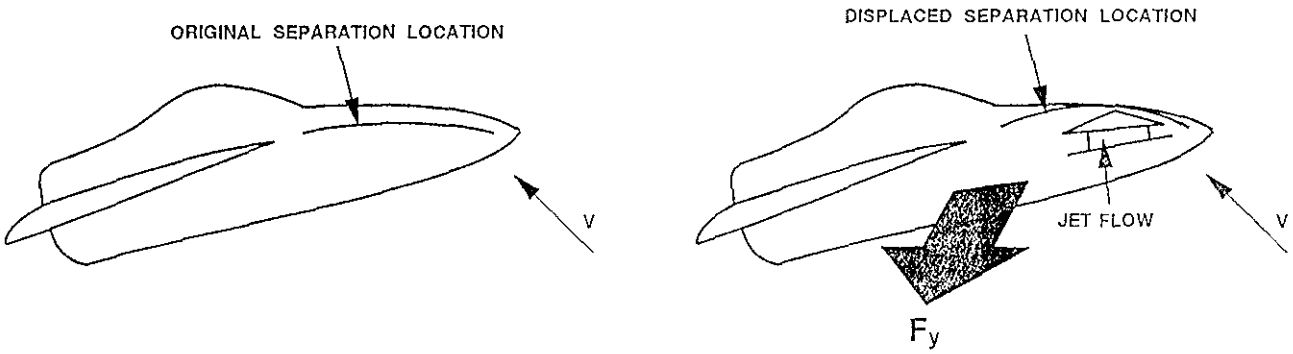

a) Without blowing b) With tangential slot blowing

Fig. 1. Schematic of forebody pneumatic control concept

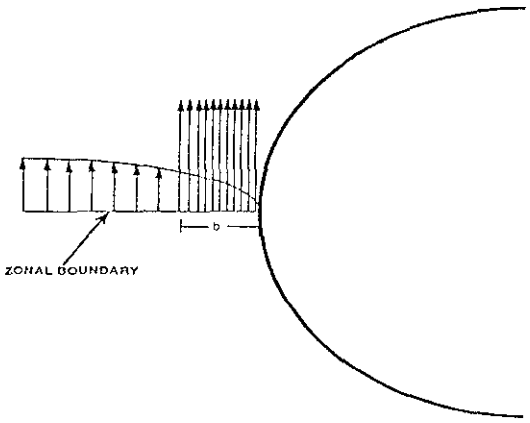

Fig. 2. Schematic of actuator plane concept

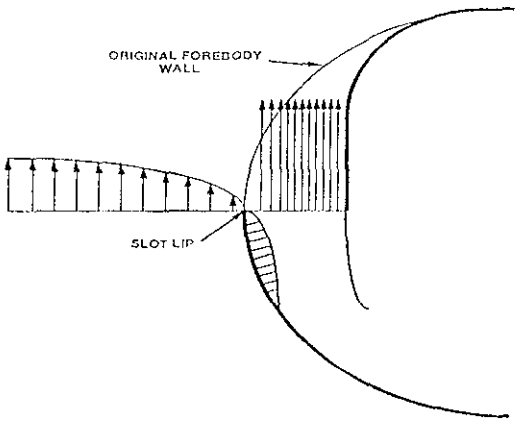

Fig. 3. Schematic of slot geometry resolution

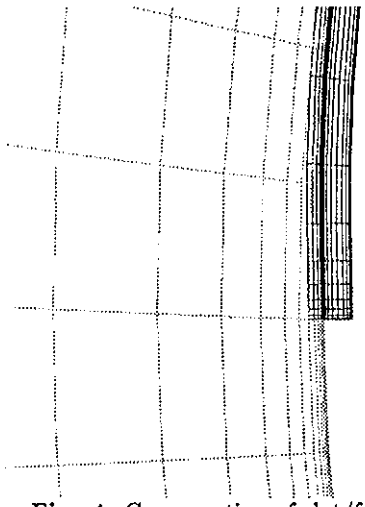

Fig. 4. Cross-section of slot/forebody grid overlap

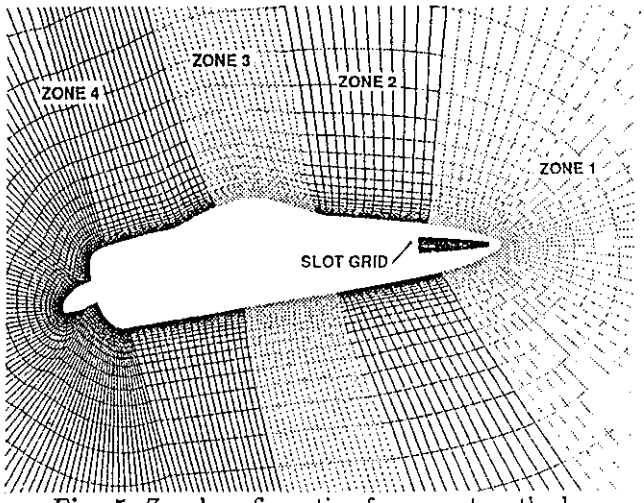

Fig. 5. Zonal configuration for overset method

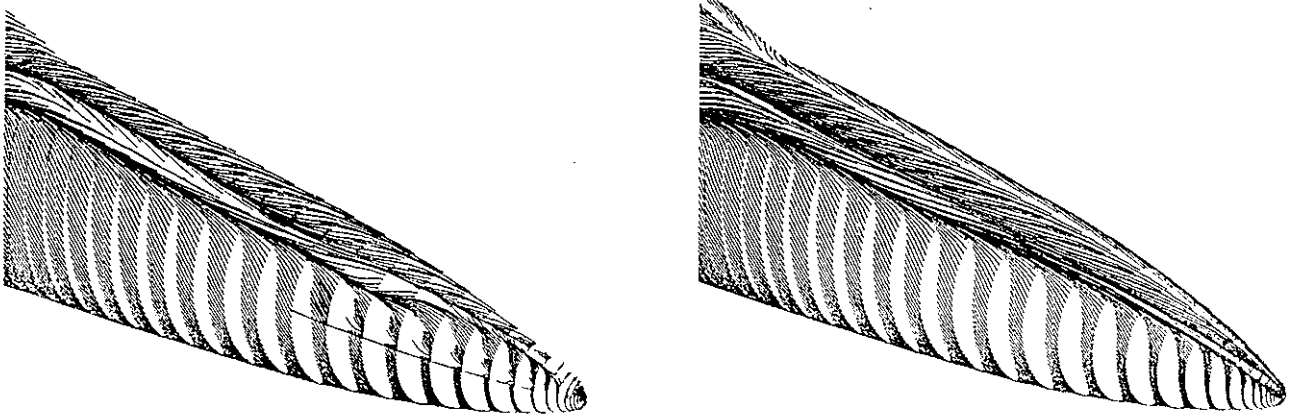

a) With $b = 0.17$ in. slot geometry b) Without slot geometry

Fig. 6. Closeup of no-blowing surface flow pattern near the nose

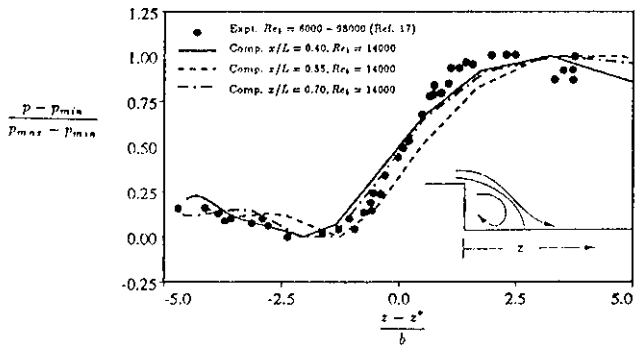

Fig. 7. Similarity pressure distribution in slot region without blowing

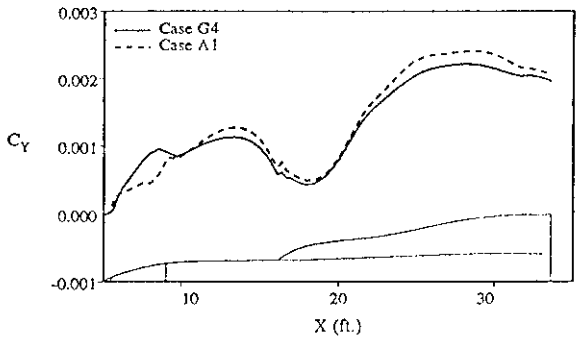

Fig. 8. Side force distribution

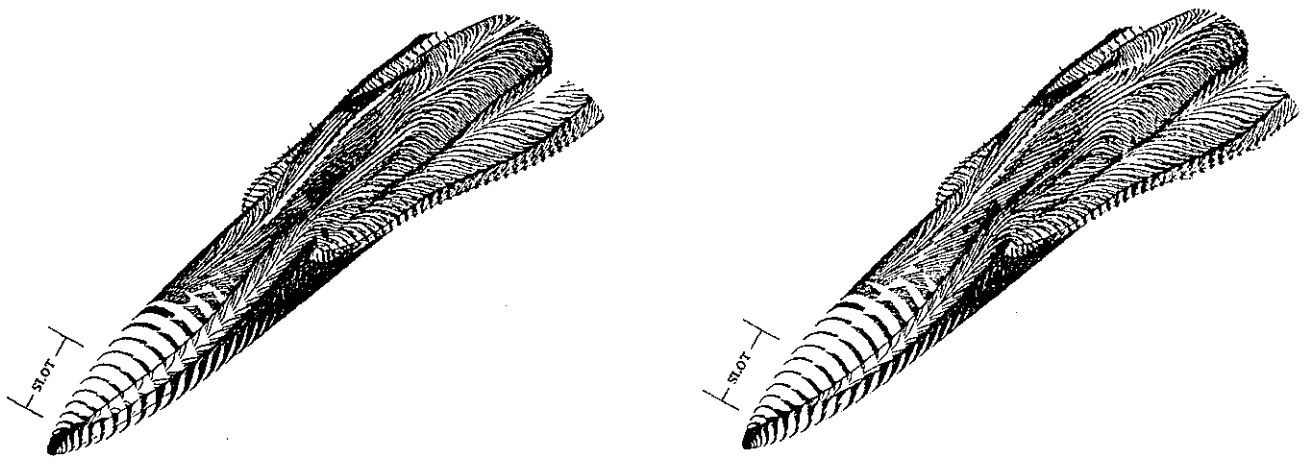

a) Case G4 b) Case A1

Fig. 9. Surface flow pattern comparison - overset vs. actuator

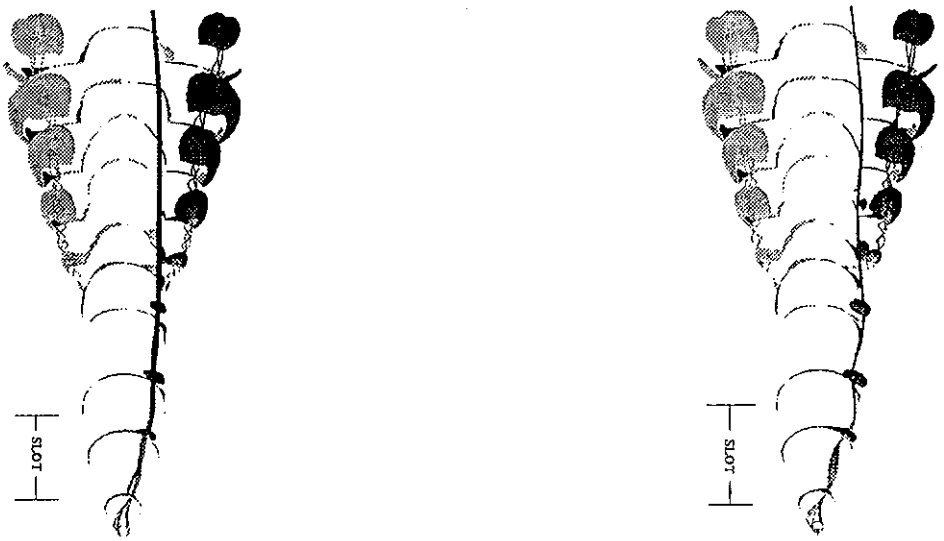

a) Case G4 b) Case A1

Fig. 10. Off-surface flowfield comparison - overset vs. actuator

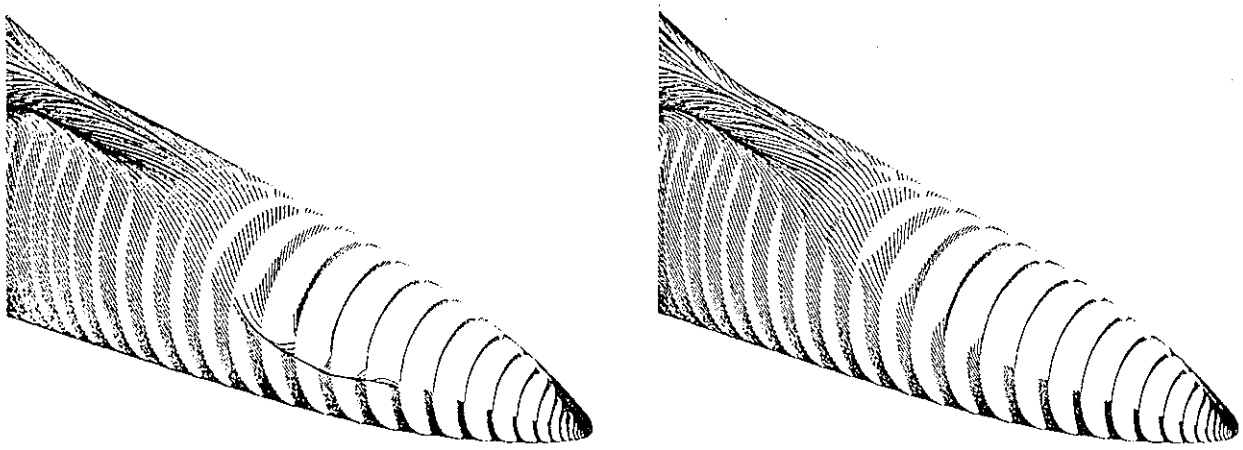

a) Case G4 b) Case A1

Fig. 11. Surface flow pattern at jet implementation - overset vs. actuator

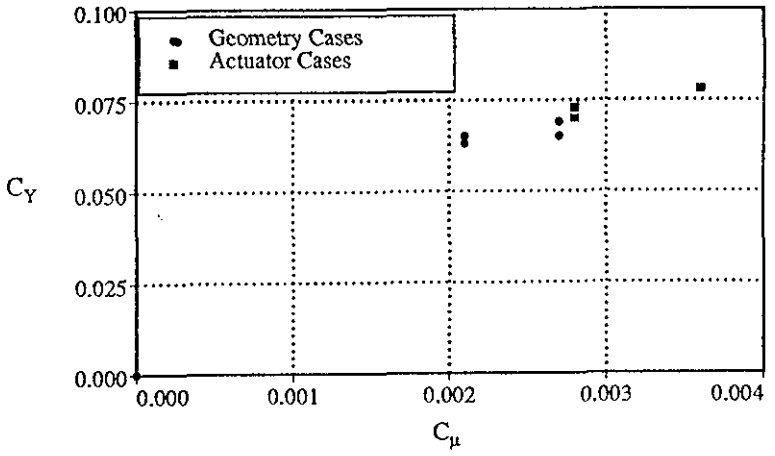

Fig. 12. Variation of side force with blowing coefficient

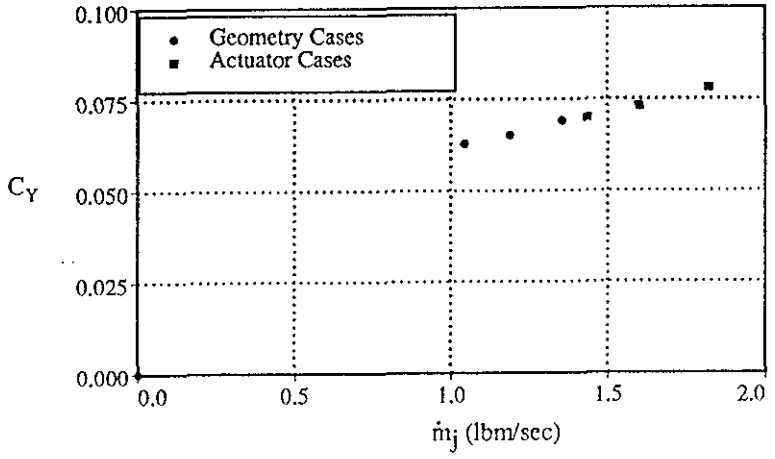

Fig. 13. Variation of side force with jet mass flow rate

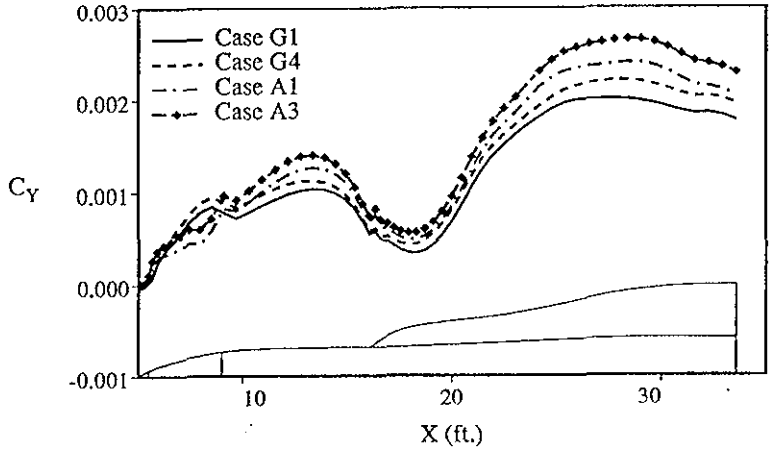

Fig. 14. Side force distribution